Final Draft
of the original manuscript:

Srinivasan, P.B.; Blawert, C.; Dietzel, W.:

Effect of plasma electrolytic oxidation treatment on the corrosion and stress corrosion cracking behaviour of AM50 magnesium alloy

In: Materials Science and Engineering A (2008) Elsevier

DOI: 10.1016/j.msea.2008.04.031

Effect of plasma electrolytic oxidation treatment on the corrosion and stress corrosion cracking behaviour of AM50 magnesium alloy

P. Bala Srinivasan*, C. Blawert, W. Dietzel
Institute of Materials Research
GKSS-Forschungszentrum Geesthacht GmbH
D21502 Geesthacht, Germany

*Corresponding Author (bala.srinivasan@gkss.de);
Phone: 00-49-4152-871997; Fax: 00-49-4152-871909

Key words:
Magnesium alloy; Plasma electrolytic oxidation; Electrochemical behaviour; Stress corrosion cracking; Fractography

Abstract

The effect of a silicate based plasma anodization treatment on the corrosion and stress corrosion cracking behaviour of a cast AM50 magnesium alloy was studied. Electrochemical tests revealed the beneficial effect of the plasma electrolytic oxidation (PEO) in improving the corrosion resistance of the alloy. Although the coating had provided an improved resistance to stress corrosion cracking in this test environment at a nominal strain rate of 10^{-6} s^{-1}, it could not completely eliminate the SCC susceptibility of the alloy. Cracking of the coating under conditions of straining was found to be the reason for SCC of PEO coated alloy.

Introduction

The light weight, combined with good mechanical properties of magnesium alloys make them candidate materials for structural, automotive and aerospace applications. Although the general corrosion behaviour of magnesium alloys with controlled levels of impurities has been reported to be better than that of aluminium and steel in some environments **[1]**, there remains a concern about their corrosion resistance. This stems from the fact that the impurities, viz., iron, copper, etc., even marginally above the threshold levels, could be harmful to the corrosion resistance of magnesium alloys. Essentially to overcome those issues, surface modification becomes mandatory, and a variety of treatments have been attempted by researchers **[2-7]**, amidst which the plasma electrolytic oxidation (PEO) treatment is becoming increasingly popular in the last few years **[8-11]**. The other major problem associated with magnesium alloys is their susceptibility to environmentally assisted cracking **[12-14]**. Some of the well known and proven alloys have been reported to be susceptible to stress corrosion cracking (SCC) even in very mild environments such as distilled water **[15]**. However, as the surface treatments improve the corrosion resistance, there may be an effect on

the SCC behaviour, e.g. by reducing the pitting and hydrogen formation – the possible sources of SCC. There seems to be not much of published information addressing the aforementioned issue, and this work is an attempt to understand the influence of PEO coatings on the stress corrosion cracking behaviour of a cast magnesium alloy.

Experimental

A cast magnesium alloy of grade AM50 with a nominal composition of 5%Al, 0.5%Mn and balance Mg was employed in this investigation. Specimens of size 30 mm x 30 mm x 5 mm were ground successively with 320, 500, 800, 1000 and 2500 grit emery sheets prior to the PEO treatment. The PEO treatment was carried out using a simple DC power supply source of 600 V and 4 A capacity. The specimens were PEO coated in an electrolyte constituted by equal weight fractions of sodium hydroxide (10 g l^{-1}) and sodium silicate (10 g l^{-1}) in double distilled water. The PEO treatment was performed at a constant current density of 15 mA cm^{-2}, to a final voltage of 420 V. The electrolyte was stirred using a magnetic stirrer, and the temperature of the electrolyte was maintained in the range 20 $\pm$ 5°C.

During the plasma electrolytic oxidation process the voltage was observed to increase rapidly upon impressing the current. The first discharges and the sparking, which are known to be dependent on the electrolyte composition, were observed at around 240V in this electrolyte. The sparks were very fine and evenly distributed across the surface of the specimen until a voltage of around 400 V. From that point onwards, the spark intensity was stronger, with an increase in size and reduction in number. The treatment was continued to a voltage of 420 V and was dwelled at that point until the current dropped down close to zero.

The phase composition analysis of the coating was done by Bruker XRD with Cu-Kα radiation. Electrochemical measurements were made using an ACM Gill AC potentiostat/ galvanostat FRA, employing a three electrode cell. The corrosion potential of the specimens was measured for a period of 1800 s before performing the electrochemical tests. Electrochemical impedance measurements were performed with an applied amplitude of $\pm$10 mV in the frequency range of 0.1 Hz to 30000 Hz at free corrosion potential. Potentiodynamic polarisation studies were carried out at a sweep rate of 0.5 mV s^{-1}, starting at -200 mV relative to the open circuit potential. The uncoated specimens were prepared by polishing up to 2500 grit emery for the

electrochemical studies, while the PEO coated specimens were used in the as-coated condition. Experiments were made in duplicate for ascertaining the reproducibility, and all the experiments were performed at ambient temperature (21 ± 2°C), in as-prepared, non-deaerated ASTM D1384 solution containing 148 mg Na_2SO_4, 165 mg NaCl and 138 mg $NaHCO_3$ in one liter of double distilled water. To understand the effect of chloride ions on the corrosion behaviour of the PEO coated specimens, electrochemical tests were also performed in an electrolyte with higher chloride concentration, viz., 0.1M NaCl. Corrosion rate measurements were made by Tafel extrapolation technique, and the point of intersection of cathodic slope at the corrosion potential was reported as corrosion current density for all the cases.

Tensile specimens with a gauge length of 10 mm and diameter of 5 mm were used for the slow strain rate tensile (SSRT) tests, the geometry of which is shown in **Figure 1**. The SCC tests were performed in ASTM D1384 test solution by following the ISO standard 7359—Part 7 **[16]**. The SSRT tests, both in air and in environment, were performed at a nominal strain rate of 10^{-6} s^{-1}. In SSRT tests in air, the specimen elongation was measured using a clip-on gauge in addition to the employment of two linear variable displacement transducers (LVDT) attached to the specimen grips. The tensile specimens, after the SSRT tests, were examined in a Heerburgg Wild M3B stereo microscope, and the fracture surface analysis was done in a Cambridge Stereoscan 2100 scanning electron microscope.

Results and Discussion

Microstructure

An optical micrograph of the AM50 alloy in the as-cast condition is shown in **Figure 2**. The coarse grain structure is on account of the conditions of casting (gravity cast), and the random distribution of the secondary phase ($Mg_{17}Al_{12}$) in the matrix is evident in the micrograph.

The coating was smooth and the thickness of the coating was observed to be around 12 µm. The scanning electron micrograph of the PEO coated surface shown in **Figure 3** reveals the presence of fine pores of diameter possibly 5 µm and below. The coating formed on the surface as a result of melting and solidification at the plasma discharge conditions is clearly seen in the micrograph. XRD measurements revealed that this layer was constituted essentially of MgO, Mg_2SiO_4 and $MgAl_2O_4$.

Electrochemical behaviour

The electrochemical impedance behaviour of the untreated and PEO coated specimens in ASTM D1384 solution and 0.1 M NaCl solution are depicted in **Figure 4**. The low electrical conductivity of the ASTM D 1384 solution on account of low concenrations of chloride, sulphate and carbonate (only in ppm level), gave rise to the registry of high solution resistance (R_s) values in the order of 1000 ohm cm². The PEO coating was found to significantly influence the corrosion behaviour, providing impedance values of around 5×10^5 ohm cm², compared to about 5×10^3 ohm cm² for the untreated alloy.

In 0.1 M NaCl solution, on account of the relatively higher electrical conductivity, a much lower R_s value was registered (compared to that in ASTM D1384 solution) for the untreated alloy. However, the R_s value could not exactly be assessed for the coated specimens as the freqency range chosen was not large enough in the high frequency domain. The impedance values for the untreated and PEO coated specimens were 1.25×10^3 ohm cm² and 2.6×10^5 ohm cm², respectively, in this test electrolyte.

The potentiodynamic polarisation behaviour of the untreated and PEO coated specimens observed in the aforementioned test electrolytes are depicted in **Figure 5**, and the electrochemical data are presented in **Table 1**. The corrosion potential of the untreated specimen was nearly the same in both test electrolytes. However, the corrosion current density value in the 0.1M NaCl test solution was apparently higher. A closer look at the anodic regions of this plot would suggest that the untreated alloy undergoes active dissolution in 0.1 M NaCl solution. On the other hand, in the ASTM D1384 solution, the increase in current was not so steep, which is attributed to the formation of a film on the surface, retarding the flow of current. No pitting was observed. In 0.1 M NaCl solution, it is evident from the anodic part of the polarisation plot and from the corrosion morphology on the specimen surface that the relatively higher concentration of chloride ions was responsible in preventing the formation of a dense protective film by way of pitting. The pitting of the specimen at the corrosion potential was also noticed in the impedance measurements, reflected as an inductive loop in the Nyquist plot (not shown), also as dipping slope in the Bode plot (Figure 4) at frequencies <1 Hz.

The behaviour of the PEO coated specimen, too, was distinctly different from the untreated counterparts in these electrolytes. The PEO coated specimen in the ASTM

test solution exhibited a more noble potential and a very similar anodic behaviour (without any signs of pitting) as observed for the untreated specimen in this electrolyte. The PEO coated specimen in 0.1 M NaCl solution showed a marginally higher potential than the untreated specimen in this electrolyte. The corrosion current density values were nearly the same for the PEO coated specimens in both the test electrolytes and were by three orders of magnitude better than their untreated counterparts. Further, the PEO coating was found to provide some resistance to breakdown in 0.1 M NaCl, and the onset of pitting was observed at a potential around -1230 mV vs. Ag/AgCl. The anodic behaviour of the PEO coated specimen was nearly similar to that of the untreated specimen after the point of breakdown, which is essentially on account of chloride ions preventing repassivation. The scanning electron micrographs of the PEO coated specimen after the polarisation test presented in **Figure 6** reveal the morphology of pits on the PEO coated surface. The above data suggest that even though the PEO coating can offer a very good general corrosion resistance, it is susceptible to localized damage in solutions containing higher concentrations of chloride ions.

Stress corrosion cracking

The stress vs. strain plots of the untreated and PEO coated specimens obtained at a nominal strain rate of 10^{-6} s^{-1} in the tests in air are presented in **Figure 7**. There was a marginal drop in the ultimate tensile strength and elongation to fracture in the PEO coated specimen. The early formation of cracks in the brittle PEO coated surface and their subsequent growth into the bulk could well be the reason for the reduction in elongation/ductility. The marginal difference in the strength level is plausibly on account of a lower degree of work hardening in the PEO coated specimen during uniaxial pulling due to the earlier fracture. Both the untreated and PEO coated specimens, however, had exhibited a near-similar reduction in cross section area values of around 12%.

The surface of the PEO coated specimen after tensile testing was observed to have fine intermittent cracks, connecting the pores developed by the PEO processing **(Figure 8)**. Despite being an integral conversion coating, the PEO layer was observed to have been flaked-off in some regions close to the fracture as can be seen in Figure 8. The macroscopic appearance of the fracture surfaces of both the untreated and PEO coated specimens was nearly the same in **Figures 9(a), (b)** and **(c), (d)**. The higher magnification fractograph in **Figure 9(e)** clearly suggests that the fracture was ductile, with fine dimples and fibrous appearance. The analysis thus suggests that the PEO

coating had a very little influence on the strength; however, it did not significantly hamper the ductility of this alloy in tests in air.

The untreated and PEO coated specimens were assessed for their stress corrosion cracking behaviour in ASTM D1384 solution by SSRT tests at a strain rate of 10^{-6} s^{-1}. Even though the SCC susceptibility of magnesium alloys is reported to be brought out more clearly at much lower strain rates (10^{-7} s^{-1} and below) **[17]**, the experiments in this investigation were performed intentionally at 10^{-6} s^{-1} to understand the effect of PEO coating on the SCC behaviour. It is to be pointed out here that the displacement was measured using LVDTs connected to the specimen grips, and hence the measured values do not represent the true elongation of the specimen. The untreated specimen endured the test only for about 35 hours at this strain rate, and failed at a stress level of 105 MPa with a strain value of around 7%, as could be seen in **Figure 10**. On the other hand, the PEO coated specimen failed after 52 hours, at a stress level of 160 MPa and a strain value of 17%. A comparison of this data with the tests in air suggest that the PEO coated specimen in ASTM D 1384 solution had registered strength and elongation levels closer to those observed in air, despite of showing SCC. This suggests that the untreated alloy has a higher susceptibility to cracking than the PEO coated one in this environment.

Optical macrographs of the SSRT tested untreated and PEO coated specimens presented in **Figures 11(a)** and **(b)** show the condition of the surface after the tests. The PEO coated specimen did show a noticeable difference in reduction in cross sectional area compared to the untreated specimen. The exterior surface of this specimen contained numerous micro cracks, essentially on account of cracking of the PEO coating due to straining during the test. This was very similar to that observed in the tests in air, but the crack sizes were significantly larger compared to those noticed in that case. A closer look at the untreated specimen surface in Figure 11(a) would reveal that this surface also had numerous micro cracks. The dissolution of the untreated alloy and $Mg(OH)_2$ formation upon exposure to the electrolyte during the SSRT test resulted in the formation of a film and apparently this film was also cracking while straining. This was very much similar to that observed for the PEO coated specimen, and even though the nature of films on the surfaces was different, the SCC in both the cases was essentially on account of cracking of the film, which had resulted in exposure of the underneath substrate to the environment, facilitating active dissolution, leading to premature failure. Also in the polarisation tests in ASTM D1384 solution no pitting was

observed in both the untreated and PEO coated specimens, and this corroborates the fact that the SCC is not originated from pitting but by the cracking of the films. The PEO coating was found to have provided an improved resistance in this test environment at this nominal strain rate of 10^{-6} s^{-1}. However, the effect of strain was very much pronounced, and failure at a much lower stress level was noticed in the SSRT test at a lower strain rate viz., 10^{-7} s^{-1} **[18]**.

The macro fractographs of the untreated and PEO coated specimens in **Figures 12(a)** and **(b)** show the differences in the fracture surface appearance. The higher magnification fractographs **(Figure 12(c)** and **(d)** of the regions marked (i) in Figures 12(a) and (b), respectively, show that the fracture was brittle and transgranular in the untreated specimen and that it was relatively ductile and fibrous in the PEO coated specimen. Even though the PEO coated specimen showed a better resistance to SCC, as reflected by the higher elongation and reduction in cross section values and also corroborated by the SEM observations, the coating could not obviate the SCC of this alloy.

Conclusions

Plasma electrolytic oxidation treatment in the silicate based electrolyte resulted in enhanced general corrosion resistance of the cast AM50 magnesium alloy in ASTM D1384 and 0.1 M NaCl solutions. Even though both the untreated and PEO coated specimens showed signs of pitting in 0.1 M NaCl solution, the PEO coating offered a better resistance to breakdown. The magnesium alloy was found to be susceptible to SCC in ASTM D1384 test solution in both the untreated and PEO coated conditions and the cracking of the film/coating under conditions of straining was responsible for the SCC. Even though the PEO coating enhanced the general corrosion resistance by many folds and offered a better resistance in the SSRT tests, it could not completely eliminate the SCC of this alloy.

Acknowledgement

The authors express their sincere thanks to Mr. Ulrich Burmester, Mr. Volker Heitmann and Mr. Volker Kree for the technical support during the course of this work. PBS thankfully acknowledges the Alexander von Humboldt Foundation, Germany, for the award of AvH research fellowship and financial assistance.

References

[1] J. E. Hillis, K. N. Reichek, High Purity Magnesium AM60 Alloy: The Critical Contaminant Limits and the Salt Water Corrosion Performance, SAE Technical Paper Series #860 288, Detroit 1986.

[2] J.D. Gray, B. Luan, Journal of Alloys and Compounds, 336 (2002) 88-113.

[3] J.E. Hillis, Proc. of 40th Annual Conf. of Metallurgists of CIM, 2001, 3-26.

[4] M. A. Gonzalez-Nunez, C. A. Nunez-Lopez, P. Skeldon, G. E. Thompson, H. Karimzadeh, P. Lyon and T. E. Wilks, Corrosion Science, 37 (11) (1995) 1763-1772.

[5] W.X. Zhang, Z.H. Jiang, G.Y. Li, Q. Jiang, J.S. Lian, Surface and Coatings Technology, (2007) doi:10.1016/j.surfcoat.2007.09.023.

[6] K.T. Rie, J. Whole, Surface and Coatings Technology, 112 (1999) 226-233.

[7] C. Blawert, D. Manova, M. Störmer, J.W. Gerlach, W. Dietzel, S. Mändl, Surface and Coatings Technology, (2008), doi:10.1016/j.surfcoat.2007.08.008.

[8] C. Blawert, V. Heitmann, W. Dietzel, H.M. Nykyforchyn, M.D. Klapkiv, Surface and Coatings Technology, 200 (2005) 68– 72.

[9] J. Liang, L. Hu, J. Hao, Applied Surface Science 253 (2007) 4490–4496.

[10] Y. Ma, X. Nie, D.O. Northwood, H. Hu, Thin Solid Films 469–470 (2004) 472– 477.

[11] C. Blawert, W. Dietzel, E. Ghali, G. Song, Advanced Engineering Materials, 8 (2006), 511–533.

[12] N. Winzer, A. Atrens, G. Song, E. Ghali, W. Dietzel, K.U. Kainer, N. Hort, C. Blawert, Advanced Engineering Materials, 7 (8) (2005) 659-693.

[13] C. Blawert, J. Swiostek, W. Dietzel, D. Letzig, A. Atrens, Proceedings of the Inzeynieria Powierzchni 2A, 2005, Corrosion 2005, Warsaw, Poland, 8-10 June 2005, 183-189.

[14] M. Bobby Kannan, W. Dietzel, R.K. Singh Raman, P. Lyon, Scripta Materialia, 57 (2007) 579–581.

[15] R.G. Song, C. Blawert, W. Dietzel, A. Atrens, Materials Science and Engineering, A399 (2005) 308-317

[16] International Standard ISO 7539, Corrosion of Metals and Alloys—Stress Corrosion Testing; Part 7: Slow Strain Rate Stress Corrosion Tests, International Organization for Standardization, Geneva, 1989.

[17] M. Bobby Kannan, W. Dietzel, C. Blawert, A. Atrens, P. Lyon, Materials Science and Engineering A (2007), doi:10.1016/j.msea.2007.07.070.

[18] P. Bala Srinivasan, C. Blawert, W. Dietzel, K.U. Kainer, Scripta Materialia, doi:10.1016/j.scriptamat.2008.02.032.

Figure Captions

Figure 1 Schematic diagram of the tensile specimen for SSRT tests
(all dimensions in “mm”)

Figure 2 Optical micrograph of the AM50 magnesium alloy

Figure 3 Scanning electron micrograph of the PEO coated surface

Figure 4 Bode plots showing the electrochemical impedance behaviour of untreated and PEO coated specimens in (A) ASTM D1384 solution (B) 0.1 M NaCl

Figure 5 Potentiodynamic polarisation behaviour of untreated and PEO coated specimens in (A) ASTM D1384 solution (B) 0.1 M NaCl

Figure 6 Scanning electron micrographs revealing the pit morphology in the PEO coated specimen after the polarisation test in 0.1 M NaCl solution

Figure 7 Stress vs. strain plots of the untreated and PEO coated AM50 alloy specimens in air

Figure 8 Scanning electron micrograph of the surface of the SSRT tested specimen (in air) showing the cracks

Figure 9 Scanning electron fractographs showing the fracture surfaces of SSRT tested specimens in air
(a) Untreated (b) PEO Coated
(c) Untreated (d) PEO Coated
(e) Fracture surface of the PEO coated specimen

Figure 10 Stress vs. strain plots of the untreated and PEO coated AM50 alloy specimens in ASTM D1384 solution

Figure 11 Optical macrographs showing the surface condition of SSRT tested specimens in ASTM D1384 solution
(a) Untreated (b) PEO coated

Figure 12 Scanning electron fractographs showing the fracture surfaces of SSRT tested specimens in ASTM D1384 solution
(a) Untreated
(b) PEO Coated
(c) Higher magnification of region (i) in 12(a)
(d) Higher magnification of region (i) in 12(b)

Table 1 Electrochemical data from the potentiodynamic polarisation tests (A) ASTM D1384 solution (B) 0.1M NaCl solution

	E_{Corr}, mV vs. Ag.AgCl	I_{corr}, mA cm^{-2}	E_{pit}, mV vs. Ag.AgCl
Untreated (A)	-1395	0.9×10^{-3}	------
PEO Coated (A)	-1273	3.4×10^{-5}	------
Untreated (B)	-1385	1.9×10^{-3}	-1380
PEO Coated (B)	-1355	1.2×10^{-5}	-1230

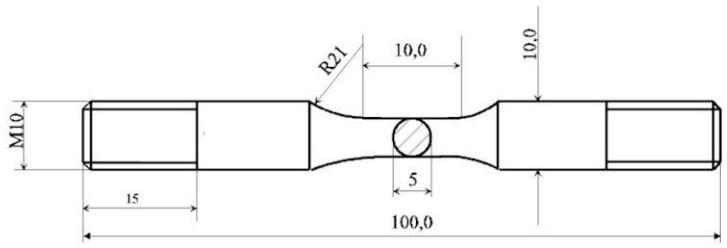

Figure 1 Schematic diagram of the tensile specimen for SSRT tests
(all dimensions in “mm”)

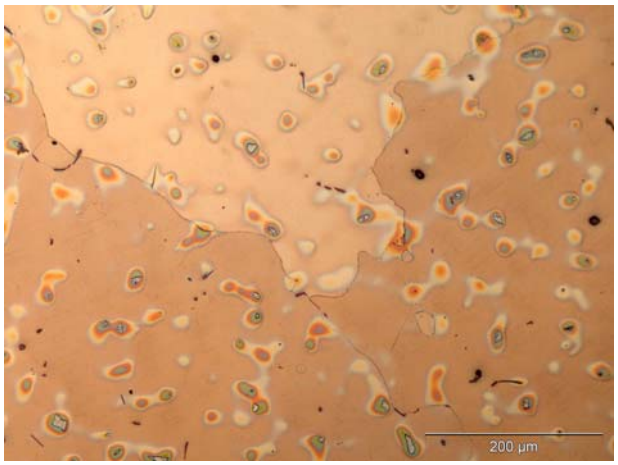

Figure 2 Optical micrograph of the AM50 magnesium alloy

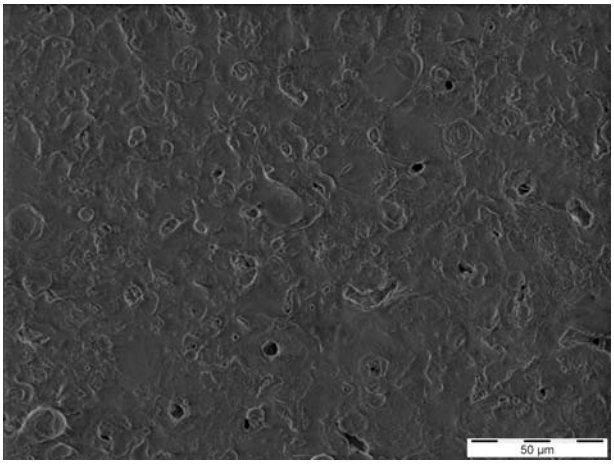

Figure 3 Scanning electron micrograph of the PEO coated surface

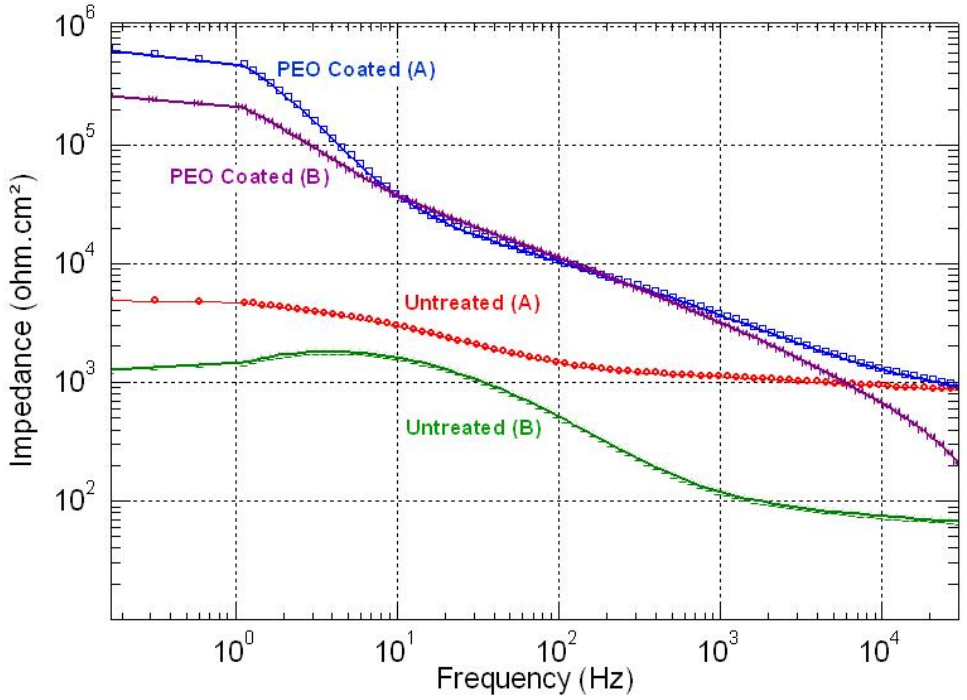

Figure 4 Bode plots showing the electrochemical impedance behaviour of untreated and PEO coated specimens in (A) ASTM D1384 solution (B) 0.1 M NaCl

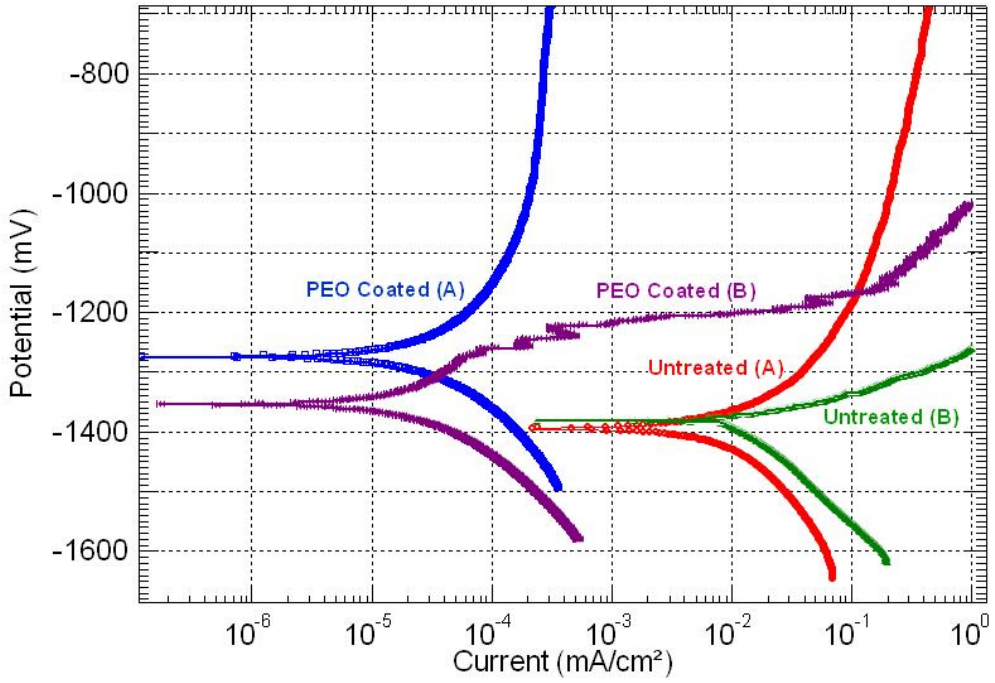

Figure 5 Potentiodynamic polarisation behaviour of untreated and PEO coated specimens in (A) ASTM D1384 solution (B) 0.1 M NaCl

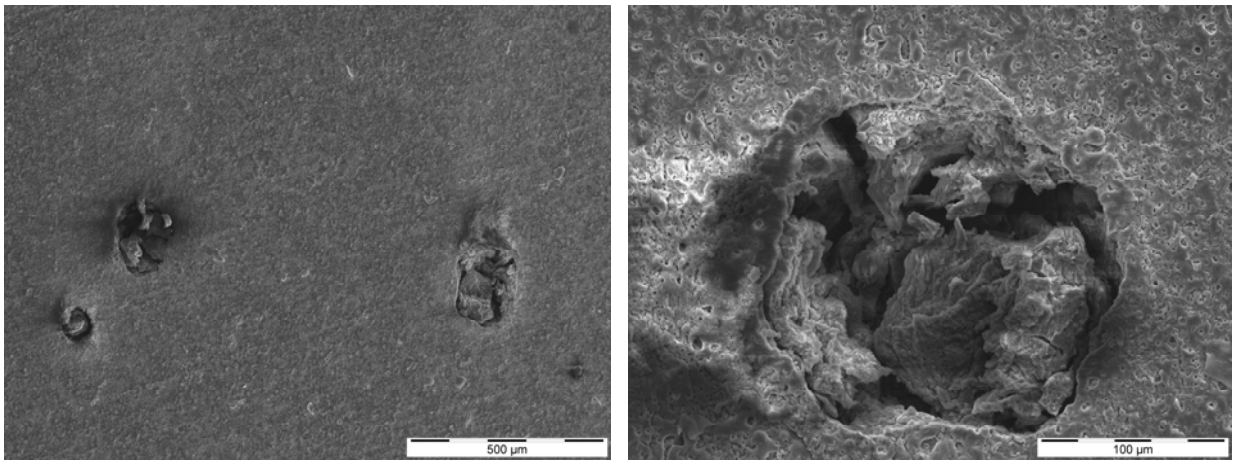

Figure 6 Scanning electron micrographs revealing the pit morphology in the PEO coated specimen after the polarisation test in 0.1 M NaCl solution

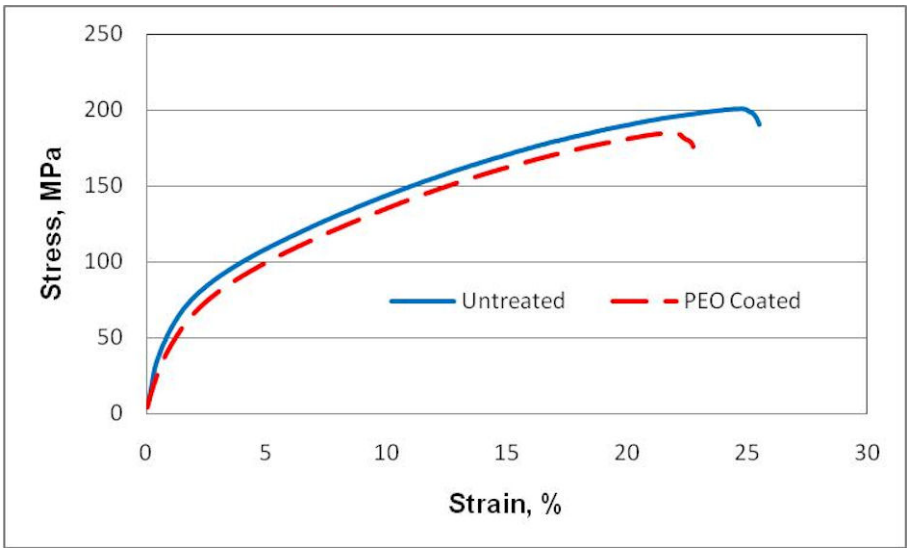

Figure 7 Stress vs. strain plots of the untreated and PEO coated AM50 alloy specimens in air

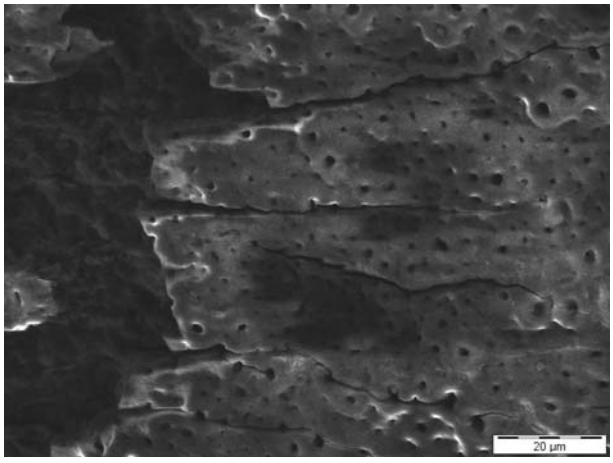

Figure 8 Scanning electron micrograph of the surface of the SSRT tested specimen (in air) showing the cracks

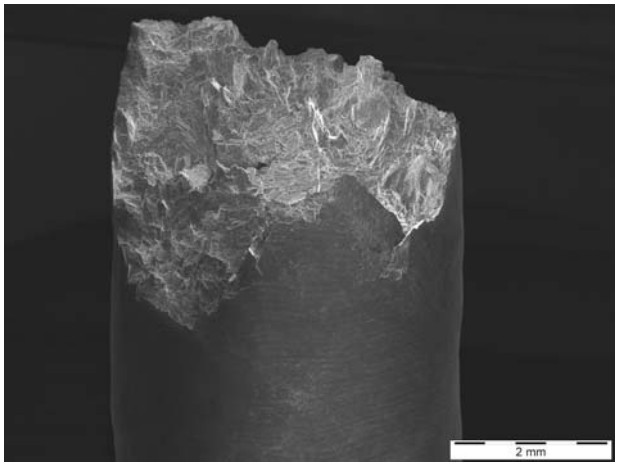

9(a)

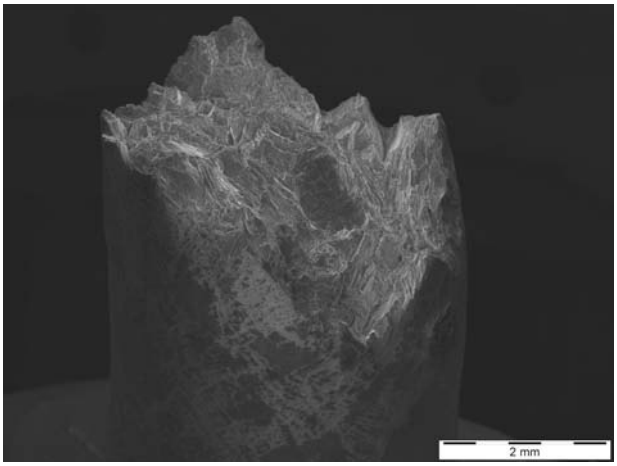

9(b)

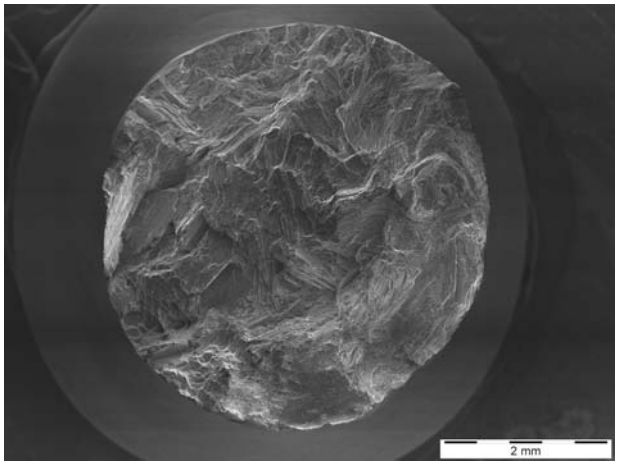

9(c)

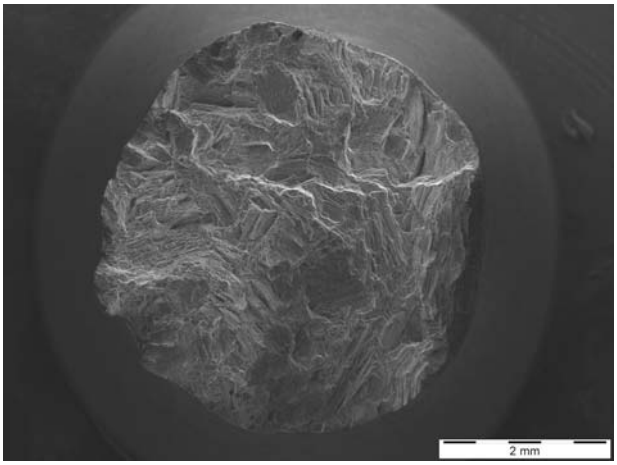

9(d)

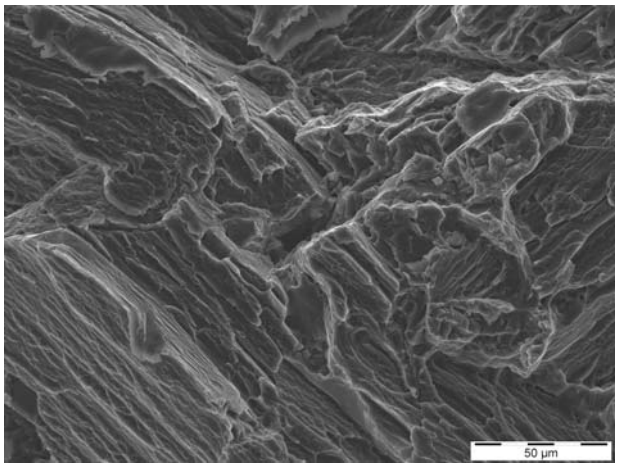

9(e)

Figure 9 Scanning electron fractographs showing the fracture surfaces of SSRT tested specimens in air

(a) Untreated (b) PEO Coated
(c) Untreated (d) PEO Coated
(e) Fracture surface of the PEO coated specimen

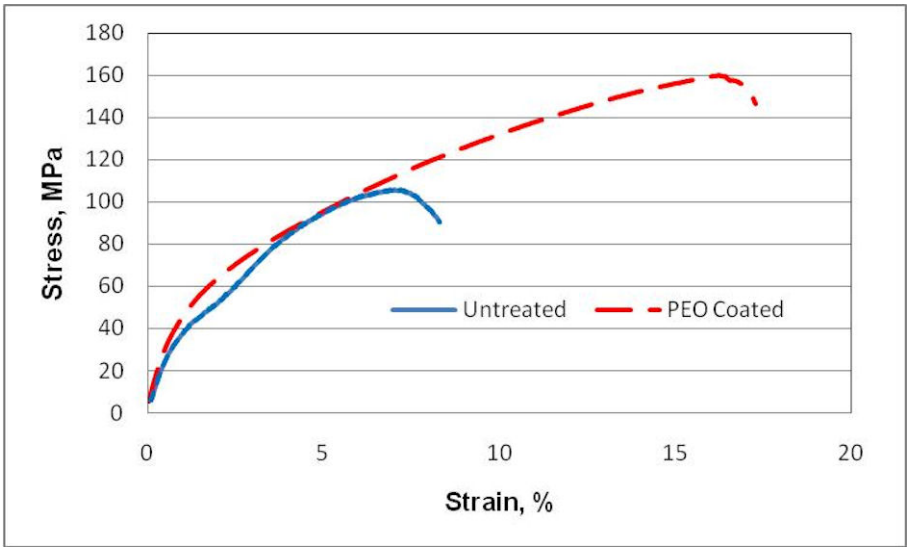

Figure 10 Stress vs. strain plots of the untreated and PEO coated AM50 alloy specimens in ASTM D1384 solution (strain rate = 10^{-6} s^{-1})

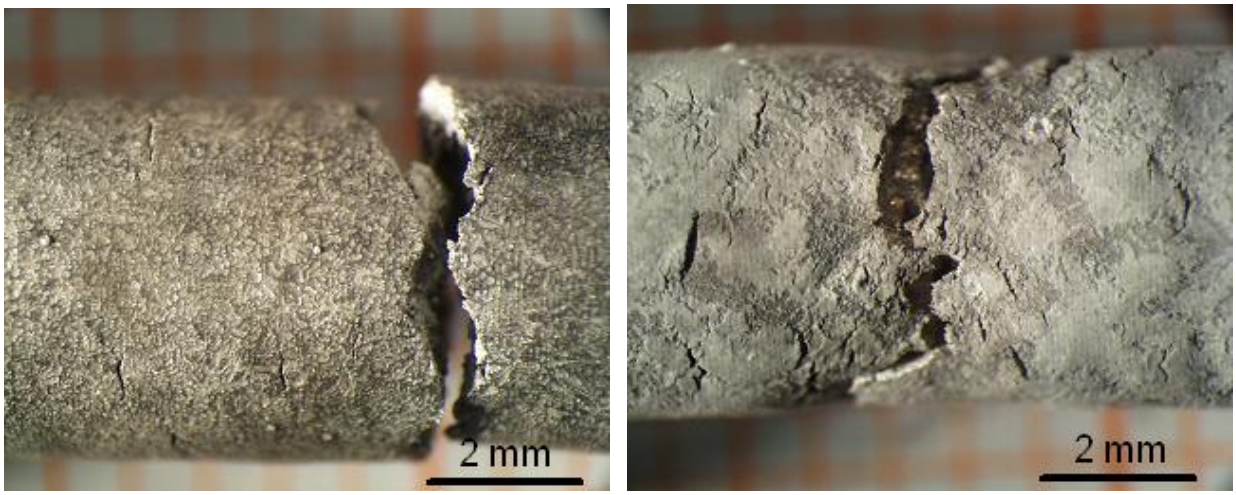

11(a) **11(b)**

Figure 11 Optical macrographs showing the surface condition of SSRT tested specimens in ASTM D1384 solution

(a) Untreated (b) PEO coated

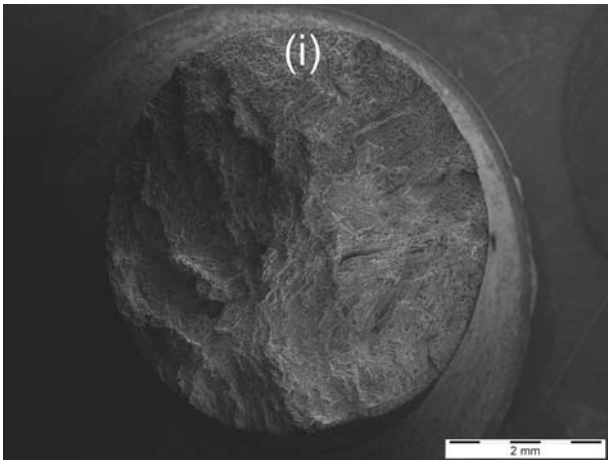

12(a)

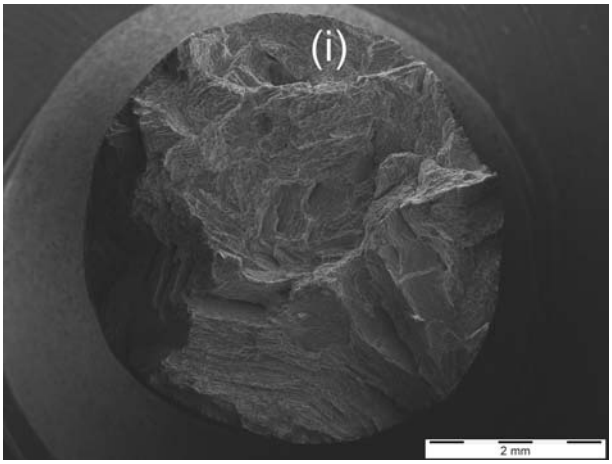

12(b)

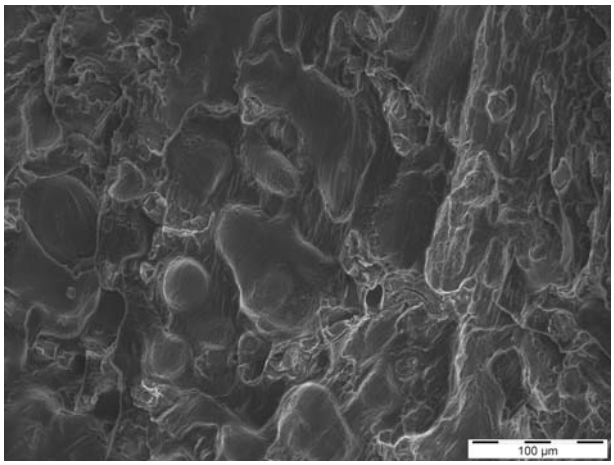

12(c)

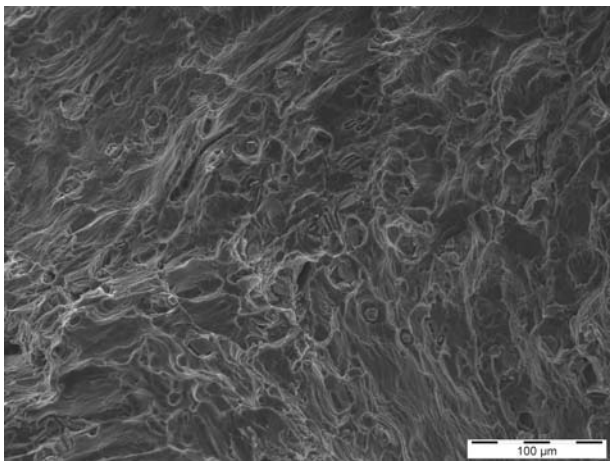

12(d)

Figure 12 Scanning electron fractographs showing the fracture surfaces of SSRT tested specimens in ASTM D1384 solution

(a) Untreated
(b) PEO Coated
(c) Higher magnification of region (i) in 12(a)
(d) Higher magnification of region (i) in 12(b)